30

Study of Turbulent Supersonic Flow Based on the Optical and Acoustic Measurements

Viktor Banakh[1], Dmitri Marakasov[1],
Ruvim Tsvyk[1] and Valeri Zapryagaev[2]
[1]*V.E. Zuev Institute of Atmospheric Optics SB RAS*
[2]*Khristianovich Institute of Theoretical and Applied Mechanics SB RAS*
Russia

1. Introduction

Aircraft and missiles moving in the atmosphere with supersonic velocities form air flows of a complicated spatial structure, in which compression shocks of different configurations and intensities arise. Since an air flow is strongly spatially inhomogeneous, the air density in the flow experiences random pulsations much exceeding turbulent pulsations of the air density in the atmosphere. Mean characteristics of supersonic flows are investigated rather well both theoretically and experimentally, but characteristic properties of turbulence in a supersonic flow are studied insufficiently.

To study turbulence in supersonic flows, the real-time measurements of the value and spectral composition of pulsations are required. Currently used sensors distort the flow structure and often have the low response rate. The dynamics of fluid or gas flows can also be studied and the turbulent velocity field in fluid and gas flows can be visualized with the use of noncontact optical methods. Among these are speckle photography and speckle interferometry methods (Fomin, 1998), in which the source of information is represented by intensity fluctuations of the laser radiation passed through the flow and a diffuse plate, as well as Doppler methods (laser Doppler anemometers (LDA)) (Abbrecht et al, 2003) and Particle Image Velocimetry (PIV) methods (Raffel et al, 2007) based on the measurement of velocities of microparticles suspended in a flow. LDA and PIV devices are very expensive and difficult in use. They are successfully used mostly for the investigation of fluid flows and subsonic gas flows. In the supersonic gas dynamics, their application is limited owing to such factors as increased requirements to the instrumentation (laser pulse energy, operation rate and sensitivity of recording instruments) and still open problems of velocity relaxation of tracing particles. In the seeding process, the tracing particle sizes are not identical and their concentration is not always uniform in a flow and this inevitably leads to the loss in accuracy of measurements.

The widely used methods of shadow visualization (Schlieren photography) do not allow the spatial spectrum of refractive index fluctuations to be determined from the obtained images. Shadow images are integral characteristics of the refractive index in the entire radiation propagation path, and the spatial distribution of the refractive index in different flow layers cannot be reconstructed from them. In this connection, it is interesting to study possibilities

of the remote diagnostics of gas flow turbulence from the intensity fluctuations of the optical radiation crossing a flow. This method does not require the presence of scattering particles and diffusors and allows the spatial structure of pulsations in a flow to be studied at dimensions of the probing beam much smaller than the flow transverse size.

In this research field, intensity fluctuations of the laser beam passed through a model plane layer of a turbulent flow and the beam propagating through a jet of a jet engine have been studied experimentally ((Joia et al, 1997, 1995) and (Dmitriev et al, 2004, Sirazetdinov et al, 2001), respectively). However, these results (Joia et al, 1997, 1995, Dmitriev et al, 2004, Sirazetdinov et al, 2001) correspond to subsonic velocities of studied flows, and for their interpretation it is sufficient to use the results of the theory of incompressible fluid mechanics (Monin & Yaglom, 1971, 1975) and optical radiation propagation in such turbulent media (Gurvich et al,1976, Zuev et al, 1988). In case of supersonic flows, for the interpretation of measured results, it is necessary to take into account not only temperature fluctuations, but also pressure fluctuations, as well as the strong spatial inhomogeneity of the flow. In recent years, the theoretical papers were published, in which the authors undertook attempts to construct an electrooptical model of parameter fluctuations in compressible gas flows (Offer Pade, 2001, 2003, 2004, 2005). However, the results obtained can be considered only as an initial stage of the study of radiation propagation in supersonic flows. In (Offer Pade, 2001, 2003, 2004, 2005), only the variance of phase fluctuations of an optical wave passed through a supersonic flow was calculated and the variance of gas density fluctuations in a flow was estimated. The calculations were based on the Fluent Dynamic 6 turbulence model.

The existing theoretical models of turbulence of compressible flows can be found, in particular, in (Yoshizawa, 1995, Smits & Dussauge, 1996, Canuto, 1997). However, in this field there is no versatile model similar to the case of developed turbulence of incompressible flows (Monin & Yaglom, 1971, 1975).

This chapter presents the results of both experimental and theoretical studies of optical turbulence in supersonic flows. The experiments on laser beam propagation through supersonic flows were conducted in T-326 and T-313 wind tunnels of the Institute of Theoretical and Applied Mechanics of the Siberian Branch of the Russian Academy of Sciences (ITAM SB RAS). The theory of laser beam propagation through a supersonic flow was based on dynamical models of the Fluent 6.0 software. The transport equations for calculation of turbulent parameters were selected according to the k-ε ring model.

2. T-313 and T-326 wind tunnels

The batch-operated T-313 and T-326 wind tunnels use compressed air for their operation. Air is compressed by high- and medium-pressure compressors at a turbocompressor station. After pre-drying, air enters high- (up to 200 bar, volume of 96 m^3) and medium-pressure (up to 18 bar, volume of 5600 m^3) cylinders. The modern automated control system provides the trouble-proof operation of the station, gathering of information about the equipment functioning and volumes of generated compressed air and circulated water (Garkucha et al., 2009).

2.1 T-313 supersonic wind tunnel

The batch-operated T-313 supersonic wind tunnel is operated since 1965 and has the closed working part with the rectangular $0.6 \times 0.6 \times 2$ m cross section (Fig. 1). The range of Mach

numbers, which can be obtained in this tunnel, is 1.75 - 7. The discrete variation of the Mach number M = 1.75, 2, 2.25, 2.5, 2.75, 3, 3.5, 4, 5, 6, and 7 is provided by replacement of hard nozzle profiled inserts.

Fig. 1. T-313 supersonic wind tunnel and the nozzle unit with changeable profiled inserts for the Mach number M =4.0.

A gas-cylinder station with the maximal air pressure up to 18 bar allows the working conditions to be maintained for about 10 min with the extreme Reynolds number $\mathrm{Re} \approx 8 \cdot 10^7\ \mathrm{m}^{-1}$ at the direct-flow operation and the Mach number of the flow M = 4. There are two air paths, namely, the cold one (direct-flow path without air heating) for the range M = 1.75-4 and the hot one for M = 5, 6, 7. A hot channel houses a 6-MW ohmic heater, which heats the air up to 500°C, thus preventing the nitrogen and oxygen condensation at a temperature decrease accompanying the adiabatic dilatation in the nozzles. A supersonic diffusor and then a two-stage ejector system are set downstream from the working part. The two-stage ejector system provides the continuous supersonic flow in the working part of the setup, decreases the load on the model during the start-up time, and allows the Reynolds number to be varied during experiments. Depending on the preset working conditions, the supersonic flow can be obtained in the working part of the setup at the operation of one or two ejectors or without ejector (direct-flow conditions).

The setup is equipped with two pressure regulation systems to maintain the preset pressure in the settling chamber at the operation in the cold or hot channel. The regulation systems are based on the application of specialized chokes moved by hydraulic actuators, which are controlled by a pneumatic hydraulic control. The air exits the gas-dynamic channel of the setup through the silencing chamber installed beyond the aerodynamic hall. Each of the two ejectors has individual regulation systems.

The setup is equipped with 4-component aerodynamic mechanic external-type weighting scales, which allow the measurement of aerodynamic characteristics of models such as resistance force, lift, pitching moment, and rolling moment. The angle of attack of the model during the test can be changed manually or automatically by a preset program in a range from –5° to +22°. The application of intramodel strain-gage weighter is possible.

To visualize the flow field near the model, the working part of the tunnel is equipped with optical windows and the coaxial IAB-451 Maksutov-system optical shadow device with the observation field 230 mm in diameter. The methods of colored oil visualization of limiting flow lines on the surface and the laser knife method are also used.

The experiments have determined that the degree of nonuniformity of the Mach number distribution in the zone of models was ~1% in the supersonic velocity range and 1.5% at hypersonic velocities. The level of mass-flow pulsations varied depending on Mach numbers from 0.27% to 0.86%.

The automation system ensures the real-time acquisition of experimental data simultaneously from a large number of channels, the graphic presentation of measured results, and the primary data processing. The multiprocessor automation system for supersonic and hypersonic periodic wind tunnels is developed in accordance with the following principles: unification of the automatic data acquisition at the level of hardware and software interfaces and the possibility of fast setting for particular experimental conditions.

The T-313 supersonic wind tunnel allows the following experimental investigations of the gas-dynamic structure of complex turbulent supersonic flows:

- Study of stationary aerodynamic characteristics of aircraft models;
- Study of the structure of detached supersonic flows with the measurement of the distribution of the average pressure and pressure pulsations on the model surface;
- Measurement of the pressure distribution in the boundary layer of the model;
- Study of the structure of supersonic flows with the use of optical visualization methods (shlieren visualization of optical inhomogeneities of the flow, laser knife method, colored oil visualization of limiting flow streamlines as a model surface is approached);
- Study of the problem of sonic boom level decrease at the flow of an aircraft flying with supersonic velocity;
- Study of interference of shock waves;
- Study of the mechanism of interaction of an intense tip vortex with a shock wave;
- Study of the interaction of supersonic jets with a supersonic wake flow;
- Study of flows in internal channels of super- and hypersonic aerojet engines, as well as study of problems of the integration of a planer and an engine of promising aircraft.

2.2 T-326 hypersonic wind tunnel

The batch-operated T-326 hypersonic wind tunnel (Fig. 2) is in work since 1971. Its working part is made as an Eiffel's test chamber.

The setup is equipped with profiled axisymmetric nozzles with a section diameter of 200 mm. The range of feasible Mach numbers is M = 6 -14. The range of Reynolds numbers is Re=(0.6 -70) · 10^6 m^{-1}. The pressure in the settling chamber is $p_0 \leq 100$ atm, the temperature in the settling chamber is $T_0 \leq 1500$ K. The wind tunnel is equipped with two air heaters. The first ohmic-type heater with power of 2.2 MW provides the Pitot temperature in the settling chamber $T_0 \leq 600$ °C and is intended to generate a flow with the Mach number M = 6-10. The second arc plasma heater with power of 1.6 MW allows the temperature $T_0 \leq 1500$ K to be achieved and is intended for investigations with $M \leq 14$. The design maximal pressure in the settling chamber is 150 bar. The measured inhomogeneity of the Mach numbers at the nozzle section in the zone of the model does not exceed 1.5%.

The tunnel is equipped with a slit ejector with the high degree of compression, which ensures the setup operation at rather small Reynolds numbers. The ejector is connected to a medium-pressure system, and the main flow comes from a high-pressure gasgolder chamber through the heater. In this setup, the hypersonic flow with the Mach number M = 6 at the nozzle section can be obtained at a pressure of 10 bar in the settling chamber. Under

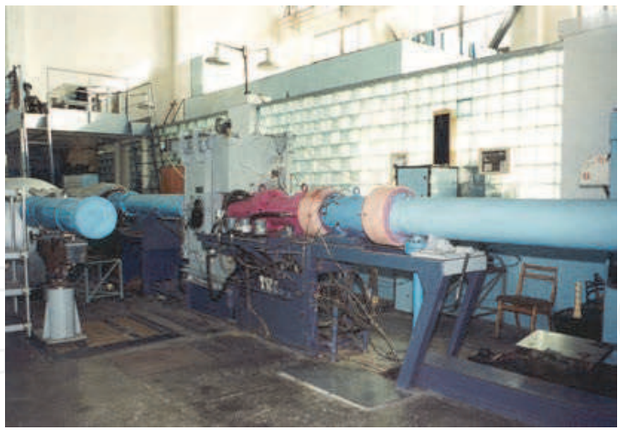

Fig. 2. T-326 hypersonic wind tunnel.

these conditions, to prevent the nitrogen and oxygen condensation in the flow, the air should be heated to the Pitot temperature no less than 400 K according to Daum recommendations.

The working part of the wind tunnel is equipped with optical windows. In addition, the wind tunnel is equipped with the IAB-451 Maksutov-system optical shadow device. The automatic data acquisition system allows one to record gas-dynamic flow parameters and readouts of pressure and temperature sensors set on the model surface.

The setup design allows one to study the shock-wave structure of supersonic anisobaric jets with the use of a specialized jet unit installed in place of the supersonic nozzle. The settling chamber of the jet unit is a tube with an inner diameter of 113 mm and has a mounting seat for changeable nozzles. The jet flows into the working chamber. The nozzle section falls within the field of view of optical windows with a diameter of 200 mm. The pointing device allows the total-pressure sensor (or other probe) to be moved in the jet flow field with the high positioning accuracy. The supersonic jet flows into the pressure chamber and is emitted into the silencing shaft through the supersonic diffusor of the exhaust line of the wind tunnel.

The T-326 hypersonic wind tunnel of the ITAM SB RAS allows the following types of experiments to be conducted: study of the laminar-turbulent transition at the hypersonic flow speed; study of heat exchange characteristics, study of flow pulsations in the anterior detachment zone; study of the structure of detached flows at the high supersonic flow speed with the measurement of the distribution of the average pressure and pressure pulsations on the model surface, as well as study of the shock-wave structure of the flow at the initial part of supersonic anisobaric jets.

3. Experimental setup for laser beam transmission through supersonic flow and acoustic measurements

3.1 Experimental setup based on T-326

Experimental investigations on the T-326 wind tunnel were conducted with the use of the jet unit with the convergent nozzle, whose section diameter was d = 30 mm. The Mach number at the nozzle section was M = 1. The pressure in the settling chamber of the jet unit was maintained so that the ratio $npr = p_0/p_c$ varied from 1.7 to 9. Here, p_0 is the pressure in the settling chamber of the wind tunnel, p_c is the pressure in the Eiffel's test chamber (0.8 × 0.8 m

working part of the wind tunnel). Some experiments were conducted on the jet unit with the vertical exit of the supersonic jet in a large room. Intensity fluctuations of the laser radiation (wavelength λ =0.63 μm) crossing the jet and the acoustic waves generated by the jet were measured in the experiments.

In the experiments, the laser radiation passed through the jet in the transverse direction at different distances x from the nozzle section along jet axis. In every cross section, the laser beam intersected the jet at different distances r from the jet axis down along the vertical. The measured results were used to calculate the relative variance and spectral functions of intensity fluctuations of the laser radiation.

The acoustic measurements were conducted in the frequency range 20 Hz-100 kHz with the use of 5 microphones 6 mm in diameter for three different configurations of microphone arrangement with respect to the jet (Fig. 3):

1. in parallel to the jet at a distance r = –135 mm from the jet axis down in the vertical direction. The measurements were conducted simultaneously by 4 microphones displaced synchronously with a step Δx = 20 mm from x = 25 to x = 245 mm;
2. around the circle 140 mm in radius (with an interval of 45°) at a distance x = 135 mm from the nozzle;
3. horizontally across the jet along the axis y in the cross sections x = 25 and 135 mm at r = -135 mm. The measurements were conducted with a step Δy = 20 mm at distances y = –30 to 110 mm from the jet axis.

The measured results were used to calculate the value and spectral density of the sonic pressure, as well as mutual correlation functions of the sonic wave between the fixed microphone and each of 4 movable microphones.

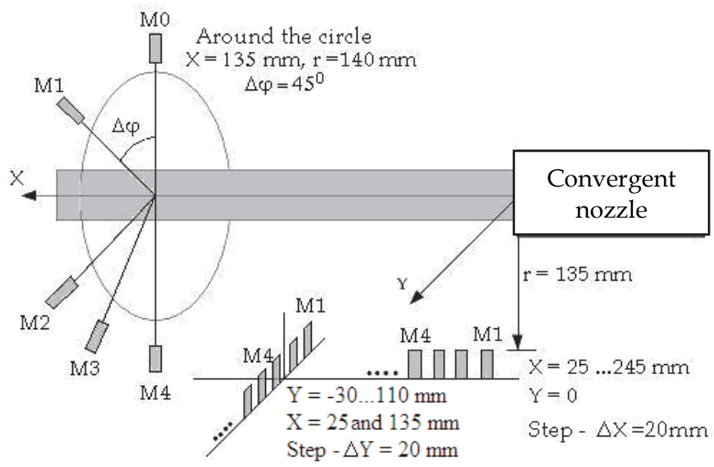

Fig. 3. Arrangement of microphones in the Eiffel's test chamber.

In some experiments, the convergent nozzle with chevrons, which changed the flow structure and, consequently, the turbulence strength and the acoustic field, were used.

3.2 Experimental setup based on T-313

In the experiments with the T-313 wind tunnel, the supersonic flow (SF) above a model of an aircraft element was studied by passing the laser beam through the flow. A plane wing model was used. The angle of attack of the wing α° (slope with respect to the SF axis)

varied from -4.7° to 19.7° toward the flow. Three lasers were used. The data recording started once the steady-state regime was established in the flow. The schematic of the optical experiments is shown in Fig.4.

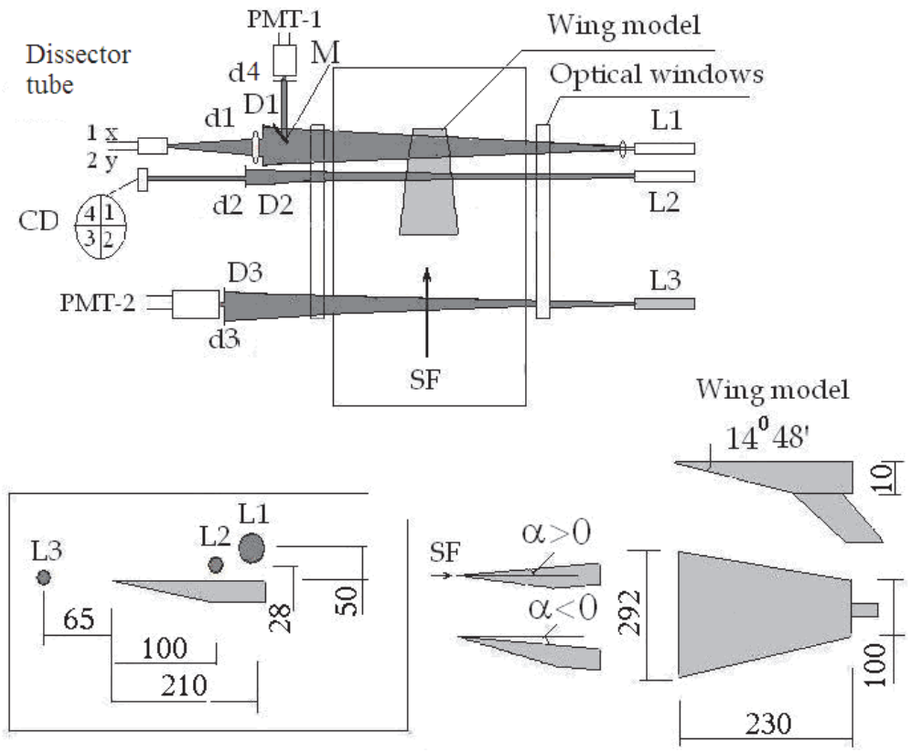

Fig. 4. Schematic of the experiment with the T- 313 wind tunnel.

The following parameters were recorded:
In front of the wing: intensity fluctuations of laser radiation in the flow incoming to the wing (photomultiplier (PMT) PMT2 and laser L3 with the beam D3 = 40 mm in diameter). The signal digitization rate was 10 MHz, the band pass of the receiving system was 0-3 MHz, and the diameter of a diaphragm set in front of the PMT was d3=0.2 mm.
Above the wing:

1. Intensity fluctuations of the laser radiation in the part of the laser beam separated by the mirror M (PMT 1 with a diaphragm d4 = 0.2 mm and laser L1 with a beam D1 = 90 mm in diameter).
2. Fluctuations of displacements of the laser beam image (system tracing the image centroid based on a dissector tube and laser L1) at the focus of an objective with a focal length of 450 mm and a diaphragm d1 = 10 mm. The signal digitization rate was 100 kHz, and the frequency range of the system was 0-1.5 kHz along every coordinate.
3. Fluctuations of the laser beam direction (four-quadrant coordinate photodiode CD and laser L2 with the beam D2 = 40 mm in diameter). The digitization rate of a signal from each element was 250 kHz. A diaphragm d2 = 2 mm in diameter was set at a distance of 700 mm in front of CD.

The data recorded were used to calculate spectral functions and relative variances of signal fluctuations.

4. Model of optical turbulence of supersonic flow

To develop a model of optical turbulence in a supersonic flow, it is necessary to know the spatial distribution of the gas density and the gas flow velocity. In addition to average values of the density and flow velocity, we also should know the characteristics of turbulent pulsations of these parameters, such as the variance and spectra of the density and the velocity components.

Average values of the flow parameters are usually determined with the system of averaged Navier—Stokes equations. The system is closed through the introduction of additional equations for the variance and the mutual correlation of fluctuations of medium parameters. There are several semiempiric models of turbulence, which allow the parameters k (turbulent kinetic energy) and ε (dissipation rate of the turbulent energy) to be calculated from the system of transport equations (Launder & Spalding, 1972, Yakhot & Orszag, 1986, Shih et al., 1995).

Within the framework of these models, we have derived the transport equation for the variance of fluctuations of the gas density $\overline{\rho'^2}$ from the equations proposed in (Yoshizawa, 1995). The equation derived looks as

$$div\left(\mathbf{u}\overline{\rho'^2}-\frac{\nu_T}{\sigma_{\rho\rho}}grad\,\overline{\rho'^2}\right)=2\frac{\nu_T}{\sigma_\rho}\left(grad\,\rho\right)^2-\left(div\,\mathbf{u}+C_D\frac{\varepsilon}{k}\right)\overline{\rho'^2} \tag{1}$$

where ρ is the mean gas density, the convective transfer of the density variance has the velocity equal to the average flow velocity vector **u**, and the turbulent kinematic viscosity ν_T serves as the diffusion coefficient. The sources in the right-hand side of Eq. (1) show that density fluctuations are generated by the inhomogeneity of the average density and gas velocity components, and the dissipation processes are determined by the dissipation of the kinetic energy of turbulent vortices (ε/k). In Eq. (1) $\sigma_\rho=\sigma_{\rho\rho}=1$ and C_D = 5.7 are constant.

In flows with velocities ~10 M and lower, the effects associated with the gas compressibility are significant for the calculation of average jet parameters, but in the turbulent component they manifest themselves only slightly (Smits & Dussauge, 1996). Therefore, the spectral distribution of density fluctuations correspond to the Kolmogorov—Obukhov model. The main parameters of the model, namely, the structure characteristic of the refractive index fluctuations C_n^2 and the inner scale of turbulence l_0 were calculated from the equations

$$l_0=\left(\nu^3/\varepsilon\right)^{1/4},\ C_n^2=1.91G^2L_0{}^{-3/2}\overline{\rho'^2}/\rho^2 \tag{2}$$

where ν is the air kinematic viscosity, G = 0.000207 is the Gladstone—Dale constant, L_0 is the outer scale of turbulence, which can be estimated from scales of spatial variations of mean values of jet parameters serving as sources of turbulence. Thus, the results of calculation of mean flow parameters based on Computational Fluid Dynamic model Fluent-6 complemented with Eqs. (1, 2) form the optical model of a supersonic jet.

In the jet in the jet module of the T326, we can see elements (barrels) formed by the characteristic configuration of density and velocity stepwise changes (hanging and reflected), the Mach disk, where the flow velocity decreases down to subsonic values, and the outer boundary of the jet. This repeated structure can be seen over several tens of

centimeters from the nozzle (4 to 5 barrels). At longer distances, the jet structure blurs due to the flow turbulization, generation of acoustic noise, and decrease of the mean flow speed down to subsonic values. The internal structure of barrels is shown in Fig. 5a. We can separate the following elements:

- Along the outer surface of the jet, there is a gradually widening mixing zone (zone 5), in which the velocity and the velocity gradient achieve their maximal values. Over the jet cross section, the mean velocity and pressure vary depending on the distance of the cross section plane from the nozzle (zones 1-3).
- Along the jet axis, the barrel-like structures repeat, their number is determined by the initial velocity of the flow. In the mean, the turbulence strength is minimal in the first barrel and grows up in the following barrels.
- The third region is the near-axis area 30-40 mm in diameter with the supersonic velocity of the flow, high pressure and density and their gradients (zones 1, 4).

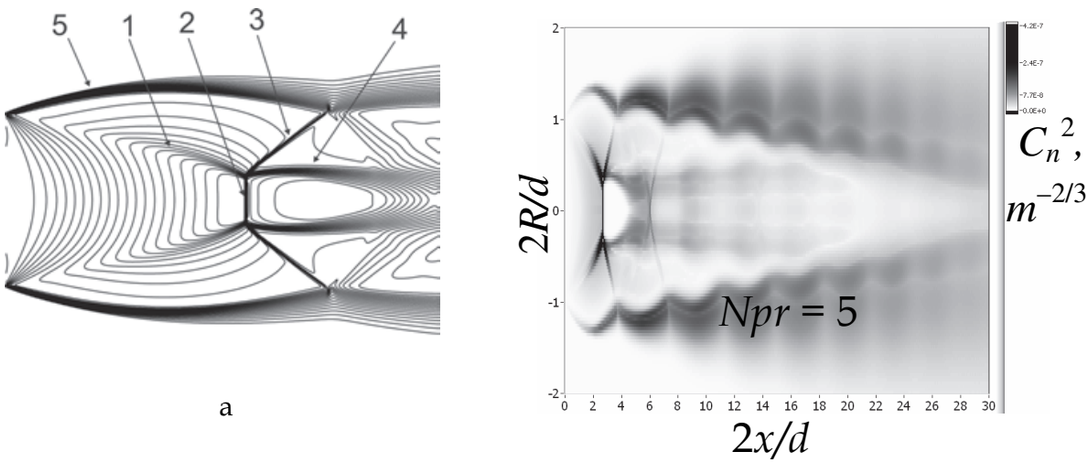

a b

Fig. 5. Structure of the air density and distribution of C_n^2 in the jet in T-326 (optical model).

To estimate perturbations induced by the supersonic flow in the optical wave propagating through it, we have simulated numerically air flows arising in the jet unit of the wind tunnel with the convergent nozzle having a diameter d = 30 mm. The calculation of turbulence parameters have shown that density fluctuations are mostly caused by stepwise changes of averaged values of parameters on the Mach disk and on the outer boundary of the jet (Fig. 5b). Near the jet axis, the turbulence is most strong in the first two barrels, where the gradients of the density and velocity components on the Mach disk and the hanging step are maximal. As the jet structure destructs with the distance from the nozzle, density fluctuations on the jet axis decrease fast. Along the whole jet, the turbulence develops on the jet outer boundary. The turbulized zone of the jet widens with the distance from the nozzle and at a distance of 20-30 cm occupies the large part of the jet cross section. In this zone, according to the results of acoustic measurements in the T-326 jet unit, acoustic noise are mostly generated. Thus, both the results of numerical simulation and the experimental findings indicate that in this zone the jet loses its kinetic energy which is expended on turbulence and acoustic noise generation.

5. Methods of computer simulation of laser beam propagation through supersonic flow and retrieval of the parameters of the flow optical turbulence

Laser radiation distortions caused by regular and random inhomogeneities of air density in the supersonic flow can be used as a source of information on optical parameters of the flow. In the general case, the problem of reconstruction of optical model parameters is a complex mathematical problem. However, for certain flow configurations it can be solved rigorously. In particular, it is possible for axially symmetric flows.

Let an axisymmetric supersonic jet propagate in the positive direction of the axis x of the Cartesian coordinate system. The laser source is at the plane $z = -l_1$, where the collimated beam with the Gaussian amplitude distribution is formed. The beam optical axis is shifted with respect to the jet axis toward the vertical axis y by the impact parameter b. The laser beam propagates through the jet and distorts at inhomogeneities of the air density in the jet. Large-scale inhomogeneities deflect the beam from the axis z, while small-scale ones distort the beam structure. A photodetector recording the beam intensity distribution in the plane $\mathbf{r} = (x,y)$ is in the plane $z = l_2$. This allows us to determine the vector of displacement of the beam energy centroid

$$\mathbf{d}(b) = \frac{\int \bar{I}(\mathbf{r})\mathbf{r}d\mathbf{r}}{\int \bar{I}(\mathbf{r})d\mathbf{r}} - b\mathbf{e}_y \tag{3}$$

which depends mostly on the distribution of the mean gas density $\rho(\mathbf{r},z)$, and the relative variance of intensity fluctuations on the beam axis

$$\sigma^2(b) = \overline{\left(I/\bar{I} - 1\right)^2} \tag{4}$$

Assuming that the beam radius is small compared to characteristic scales of variation of jet parameters, we can consider the dependence of measured parameters (3, 4) on the impact parameter b as a way to estimate the radial dependence of the mean density and the structure characteristic of the refractive index fluctuations in the jet. In many applied problems, the angles of beam deflection due to optical refraction are small ($\sim 10^{-3}$ rad), and the displacement of the probing beam energy centroid inside the jet is small as well. This allows us to obtain an approximate equation for the inversion of the refractive index dependence of the y-component of the beam energy centroid displacement vector and to find the radial distribution of the mean refractive index in the jet cross section

$$n(R,x) = \frac{1}{\pi}\int_R^\infty d_y(b)\left[(l_2^2 + d_y^2(b))(b^2 - R^2)\right]^{-1/2} db + n(\infty,x) \tag{5}$$

where $R = \sqrt{y^2 + z^2}$ is the distance to the jet axis. The mean air density in a flow is directly proportional to the mean refractive index.

For the regime of weak intensity fluctuations (Zuev et al., 1988) wich realized for the laser beam passed through the jet, we can obtain the equation analogous to Eq. (5) for the structure characteristic of the refractive index fluctuations in the axisymmetric flow

$$C_n^2(R,x) = -\frac{1}{\pi A}\int_R^\infty (b^2 - R^2)^{-1/2}\frac{\partial}{\partial b}\sigma^2(b;x)db\ , \tag{6}$$

where A is a constant determined by the position and parameters of the radiation source.
Thus, if a narrow laser beam propagates repeatedly through the jet in some cross section x and the recorded intensity distributions are then used to determine the dependence of displacements of the energy centroid of the beam and the relative variance of the intensity at the beam axis on the impact parameter, we can reconstruct the radial dependence of parameters of the optical model in this cross section using Eqs. (5, 6).
The algorithms of reconstruction of flow parameters have been tested in a series of closed numerical experiments. The geometry of the experiments corresponded to the T-326 jet unit. We considered the flow of the supersonic air jet into a half-space filled with air at an atmospheric pressure and temperature of 300 K, as well as the airflow of a conic model of an aircraft nose cone. For the simulation of the laser beam propagation, we used the method of splitting by physical factors (Kandidov, 1996). For each given cross section x, we determined the area occupied by the flow, where the parameters of its optical model differed from their background values by more than 1%. Beyond this area, we neglected atmospheric turbulence, assuming the refractive index to be unit. The flow area was divided into 30 layers of the same thickness. Perturbations introduced by each layer into the laser beam were simulated by phase screens placed at the center of the corresponding layer. At each screen, the phase of the laser beam field was distorted by regular distortions calculated from the mean value of the refractive index at the current screen point and by random additions, which had zero means and were distributed by the normal law with the power-law power spectrum corresponding to the Kolmogorov—Obukhov model of turbulence (Monin & Yaglom, 1971, 1975) for air refractive index fluctuations. The parameters of the turbulent model (structure characteristic and characteristic scales) were determined from the optical model of the flow. As a result, in each random realization the beam propagation through the jet was simulated by a series of propagation steps in vacuum between screens, where the computations were performed in the paraxial approximation, and phase perturbations at the screens. The accumulation of random realizations of the intensity distribution in the receiving plane allowed us to determine the displacement of the beam energy centroid and the variance of intensity fluctuations at the beam axis by Eqs. (3, 4). This procedure was repeated for other values of the impact parameter b, and this allowed us to find ultimately the radial distributions of the mean air density and the structure characteristic of the refractive index fluctuations in the flow through the calculation of the integrals in Eqs. (5, 6).

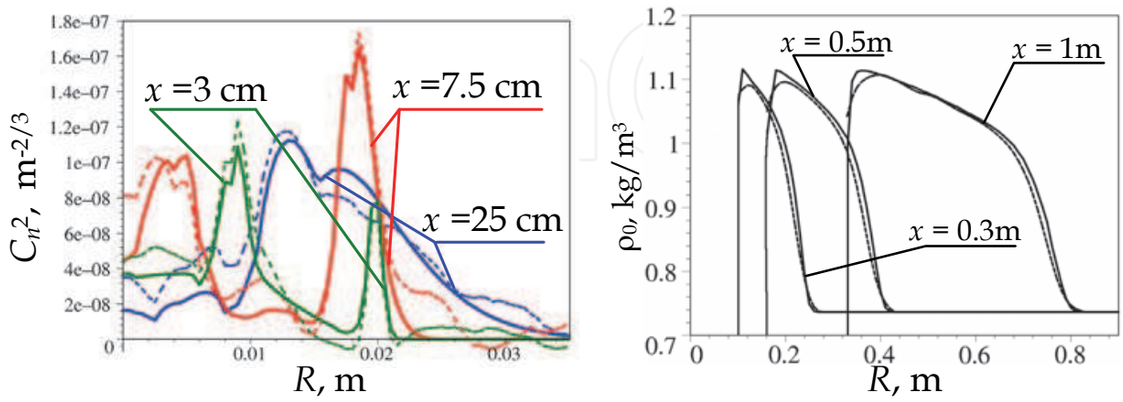

a b

Fig. 6. Initial and reconstructed radial dependences of the structure characteristic in the free jet (a) and mean density in the jet flowing over the model (b).

Figure 6 shows the results of reconstruction of parameters of the optical model for the free jet (a) and the jet flowing over the conic model (b). The good agreement between the reconstructed values and initial data of the optical model of the flow both in the region of the turbulent decomposition of the jet and at the initial part of the jet with pronounced stepwise changes of averaged parameters demonstrate the possibility of the contactless determination of supersonic jet characteristics by optical methods.

6. Experimental and theoretical study of optical turbulence in supersonic flow of the T-313 and T-326 wind tunnels

6.1 T-326 wind tunnel

The propagation of laser radiation through a supersonic jet differs significantly from the case of atmospheric propagation. In the atmosphere, mean characteristics and turbulence on the path vary quite smoothly. In the jet, to the contrary, we observe strong gradients of the mean pressure and velocity (Fig. 5), and, consequently, the density and the refractive index of air. We should also take into account the propagation of probing beam outside the jet, where the sonic waves generated by the jet can affect significantly the beam.

6.1.1 Laser radiation intensity fluctuations

First experiments on the laser beam propagation through the jet used the scheme with reflection. The laser radiation passed through the Eiffel's test chamber below the jet, reflected from a mirror 300 mm in diameter, and came back to a photodetector through the jet. The FFT method was used to calculate the spectral function $U(f)=fW(f)$, where f is frequency, $W(f)$ is the spectral density of laser radiation intensity fluctuations.

The spectra of intensity fluctuations measured at $npr = 5$ have two peaks at frequency $f_{m1} \approx$ 1000-1200 Hz and $f_{m2} \approx$ 35–60 kHz. At $npr = 9$, the spectra in the region of the second peak extend toward higher frequency. The analysis has shown that the first peak is caused by the influence of acoustic waves generated by the jet on the beam during its propagation along the path part beyond the jet. The estimates based on obtained spectra have shown that the length of acoustic waves generated by the jet was $\Lambda \approx$110.7–132.8 mm. The second peak is caused by inhomogeneities of the air density (air refractive index) in the jet.

In the further experiments, the beam path length beyond the jet was much shorter to minimize the effect of acoustic noise on intensity fluctuations of the probing beam.

Spectral functions of intensity fluctuations of the probing beam without influence of acoustic waves at different *npr* are shown in Fig.7. Figure 7b shows the spectra normalized to their values of $U(f_{m2})$ at the peak. The frequency normalized to f_{m2} is shown as abscissa. One can see from the figure that an increase in *npr* leads to a significant increase in power and to a shift of the spectrum toward higher frequencies.

At a distance $x = 15$ mm from the nozzle, the spectral peaks lie in a range $f_{m2} \sim$ 50-55 kHz, and the high-frequency part of the spectrum ($f > f_{m2}$) in the frequency range below 2 MHz drops as $\sim f^{-3.5}$. At $x > 100$ mm, the peak frequencies increase up to $f_{m2} \sim$ 70-77 kHz, and the high-frequency part of the spectrum ($f > f_m$) drops as $\sim f^{-4}$. In the low-frequency range, the spectral density increases as $\sim f^{0.8}$. The scales of inhomogeneities of intensity fluctuations of the probing beam corresponding to the frequencies $f_{m2} \sim$ 70-75 kHz are close to l = 2.4-2.5 mm.

For the nozzle with chevrons, the behavior of the intensity spectrum of the probing beam remains the same as for the nozzle without chevrons.

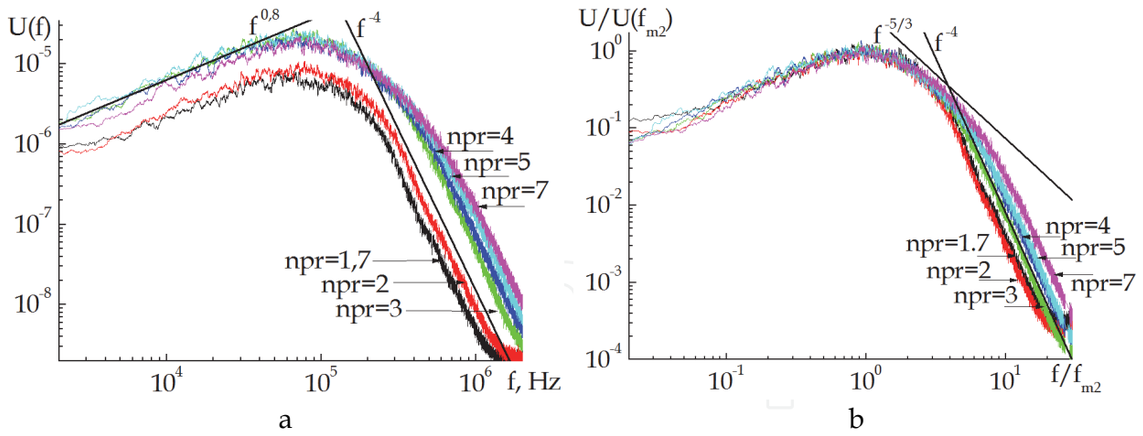

Fig. 7. Spectra of intensity fluctuations at different *npr*.

Figure 8a shows the dependence of the relative variance of intensity fluctuations of the probing beam σ^2 on the distance x along the jet axis at different distances from the jet axis r. The measurements were conducted with the use of the convergent nozzle with and without chevrons. It follows from the depicted data that without chevrons as x increases, intensity fluctuations first increase at the first two barrel-like structures up to $x \sim 100$ mm, remain at a constant level up to $x \sim 270$ mm, and then increase fast. An increase in *npr* from 1.7 to 7 leads to intensification of intensity fluctuations. The installation of chevrons increases the intensity fluctuations of the beam 6 to 8 times compared to that without chevrons in the jet part near the nozzle. As x increases, intensity fluctuations decrease.

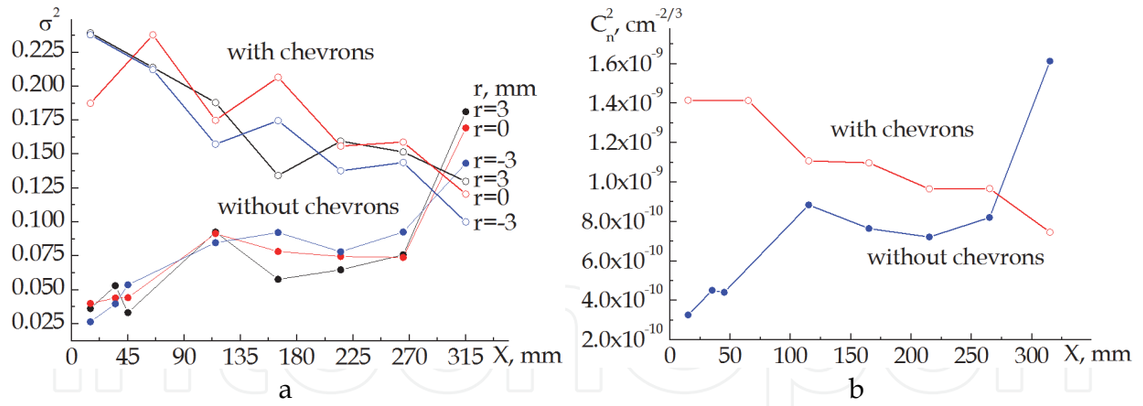

Fig. 8. Variance of intensity fluctuations along the jet axis (a), calculated values of the structure characteristic of fluctuations of the refractive index (b).

Assuming that turbulent intensity fluctuations of the probing laser beam can be described based on the Kolmogorov model of turbulence and using for the intensity relative variance σ^2 the equation $\sigma^2 = 0.46\, C_n^2 k^{7/6} L^{11/6}$ obtained in the first approximation of the Rytov method (Tatarskii, 1967, 1971) we can estimate the structure characteristic of fluctuations of the refractive index C_n^2 in the jet from measured values of σ^2. Here $k = 2\pi/\lambda$ is the wave number, L is the path length in the jet. The estimates of the average values of C_n^2 along the axis (Fig. 8b) exceed the maximal atmospheric values by 4 to 5 orders of magnitude. With

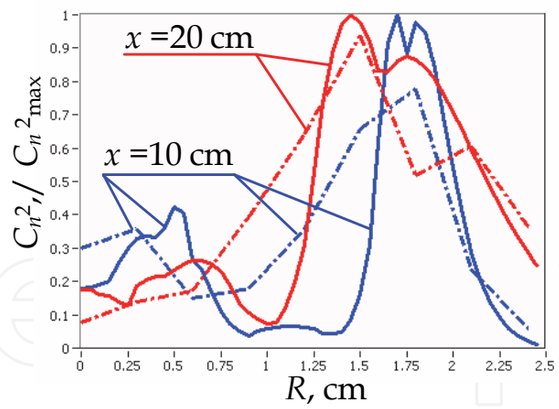

Fig. 9. Radial dependence of the structure characteristic in the jet in different cross sections calculated by the optical model (solid curves) and reconstructed from the results of laser probing (dashed curves).

the increase of x, the values of C_n^2 in the jet without chevrons increase from $3 \cdot 10^{-10}$ to $1.6 \cdot 10^{-9}$ cm$^{-2/3}$, while with chevrons they decrease from $1.4 \cdot 10^{-9}$ to $8 \cdot 10^{-10}$ cm$^{-2/3}$.
The dependence of the variance of the beam intensity measured at different distances from the jet axis was then used to reconstruct the radial dependence of the structure characteristic of the refractive index in the jet without chevrons with the use of the reconstruction algorithm (6) modified for a quickly divergent beam. The results of the reconstruction shown in Fig. 9 are in a good agreement with the dependences drawn based on the optical model of the jet.

6.1.2 Acoustic measurements

The acoustic measurements on the jet unit of the T-326 wind tunnel with the use of microphones (Fig. 3) have shown that at $npr = 5$ the sound generated by the jet had one pronounced harmonic component at the frequency $f_m \approx 3030$ Hz (Fig.10a). The Strouchal number for this frequency can be estimated as $St = fd / V_c = 0.265$, where V_c is the sound speed, d is the nozzle diameter. This estimation is close to the literature data (Kuznetsov, 2008). At $npr = 9$ there is no pronounced main harmonic, and the sound is generated in several spectral intervals.

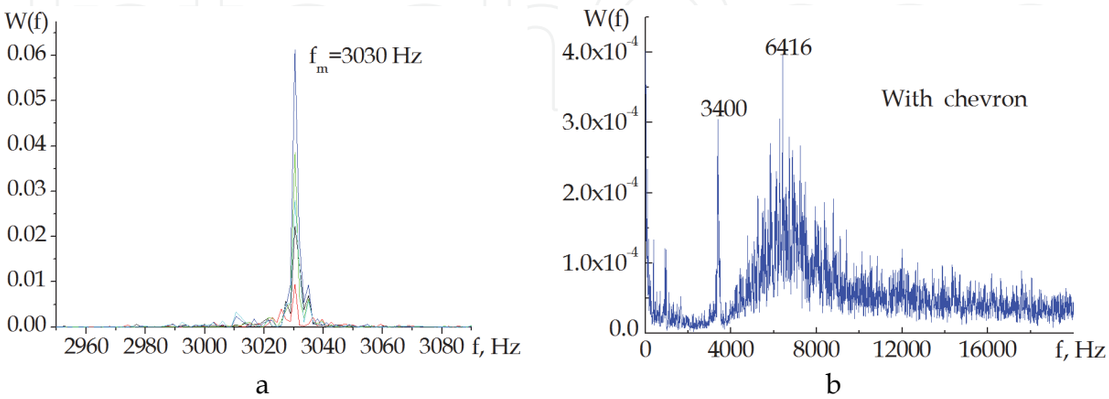

Fig. 10. Spectral power density of the sound generated by the jet at $npr = 5$ with the use of a nozzle without chevrons (a) and with chevrons (b).

If a nozzle with chevrons is used in the jet unit (Fig.10b), then the separate harmonic at the frequency f = 3400 Hz (close to the frequency of the main harmonic in the case without chevrons) remains and spectral components in a band of 4-20 kHz peaking near f = 6.4 kHz appear. The wavelength of the main harmonic at npr = 5 is roughly equal to 113 mm, and at npr = 9 it is 146 mm. For comparison, the acoustic wavelength determined from the frequency f_{m1} of the maximum of the spectral function of intensity fluctuations of the probing laser beam (Section 6.1.1.) is 110.7-132.8 mm.

To determine the form of the acoustic wave, we calculated the mutual correlation of acoustic signals measured by microphones M0, …, M4. As an example, Fig. 11 shows the coefficients of mutual temporal correlation of acoustic signals between the microphones in configuration 1 (Section 3.1, Fig. 3).

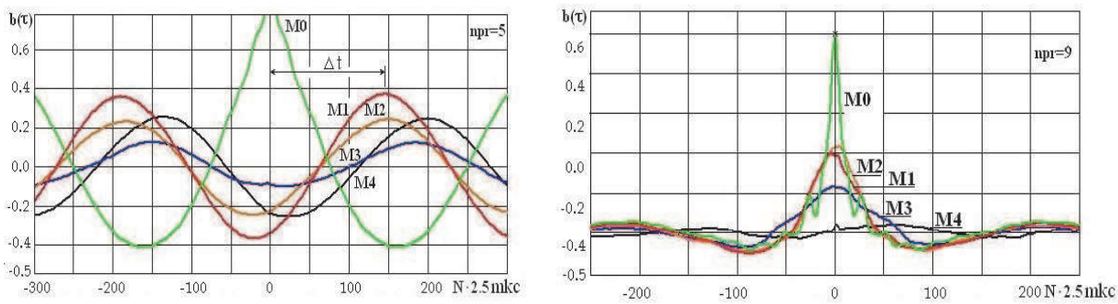

a b

Fig. 11. Time correlation coefficients of the acoustic wave: M0 is the autocorrelation coefficient of the first microphone, M1,…,M4 are the coefficients of mutual correlation between microphone M0 and microphones M1, M2, M3, M4, φ is the phase shift, N is the readout number.

It can be seen from Fig. 11 that the mutual correlation coefficients at npr = 5 vary by the harmonic law in the range 0.15–0.40 and keep their amplitude in time. This corresponds to the presence of the pronounced main harmonic in the spectrum. At npr = 9, the correlation decreases quickly with time in accordance with the noise form of the spectrum in this case.

Phase shift of the acoustic wave

The phase shift of the acoustic wave was determined from the position of the maxima of the correlation functions of M0, M1, M2, M3, M4 on the time scale, as shown in Fig. 11. The results of the determination of the phase shift at different configurations of the microphones (Fig. 3) are shown in Fig. 12.

For configuration 1, the phase shifts were determined with respect to the microphone installed at a distance of 135 mm from the nozzle. It follows from the data presented that the phase shift increases linearly as the distance to the nozzle shortens and has a minimum at a distance of 225 mm. To interpret experimental data, we have estimated the phase shift φ between the microphones on the assumption that the generated acoustic wave is spherical. The phase shift was calculated from the difference in distances ΔL between the microphone set at a distance x_0 = 225 mm from the nozzle and all other microphones (Fig. 12 *d*) by the equation

$$\varphi(x) = \pi\Delta L/\lambda,$$

where

$$\Delta L = [(x - x_0)^2 + h^2]^{1/2} - h.$$

It can be seen from Fig. 12 *a* that the calculated data are close to the experimental dependence. This suggests that the sound source is at a distance of about 225 mm from the nozzle, and at a distance of 135 mm from the jet axis the acoustic wave is close to a spherical one. The phase shift between the microphones set at distances of 225 and 25 mm from the nozzle is ≈ 2.75π or 1.4λ.

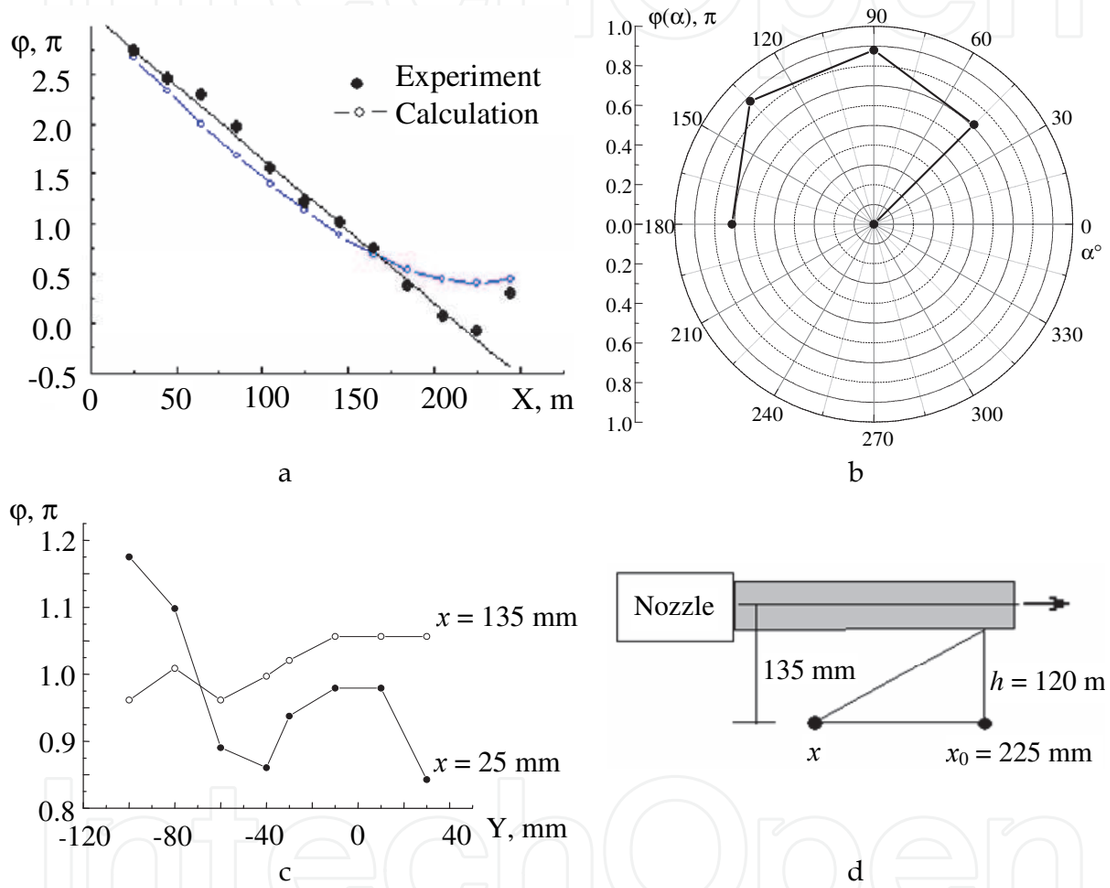

Fig. 12. Phase shift of acoustic waves at measurements with microphone configurations (Sec. 3.1) 1 (*a*), 2 (*b*), 3 (*c*) and illustration to the calculation of the phase shift (*d*).

The measurements with configuration 2 show that the phase shifts between microphone M0 and the others are close and range within 0.7–0.9π. The conclusion about the close phase shifts between the microphones is also valid for configuration 3 at measurements at a distance x = 135 mm from the nozzle. In this case, the phase shifts range within 0.95–1.05π (Fig. 12c).

Figure 13 shows the results of numerical simulation of the acoustic field generated by the supersonic jet (Bodony, 2005). It can be seen that the source of the acoustic wave is near the area of the transition from supersonic flow velocities to subsonic ones. At some distance from the source, the acoustic wave becomes close to a spherical one and the phase shift is

observed in the wave front above and below the jet. This is in a qualitative agreement with the experimental data in Fig. 12.

For the more detailed comparison, Fig. 13 shows the approximate (with respect to the simulated acoustic field) arrangement of the microphones along the jet in accordance with configuration 1 (Section 3.1) and the estimated phase of the simulated acoustic field at different distances along the jet. One can see that the phase of the acoustic wave near the beginning of the jet $\varphi = 2.7\pi$ is close to the experimental value $\varphi = 2.75\pi$ at a distance of 25 mm from the nozzle. The arrangement of the microphones was determined with respect to the nozzle diameter d (see Fig. 13) so that r/d and x/d to be equal to the experimental data x/d=85/30 (φ=2π), x/d=225/30 (φ=0), x/d =25/30 (φ=2.7π).

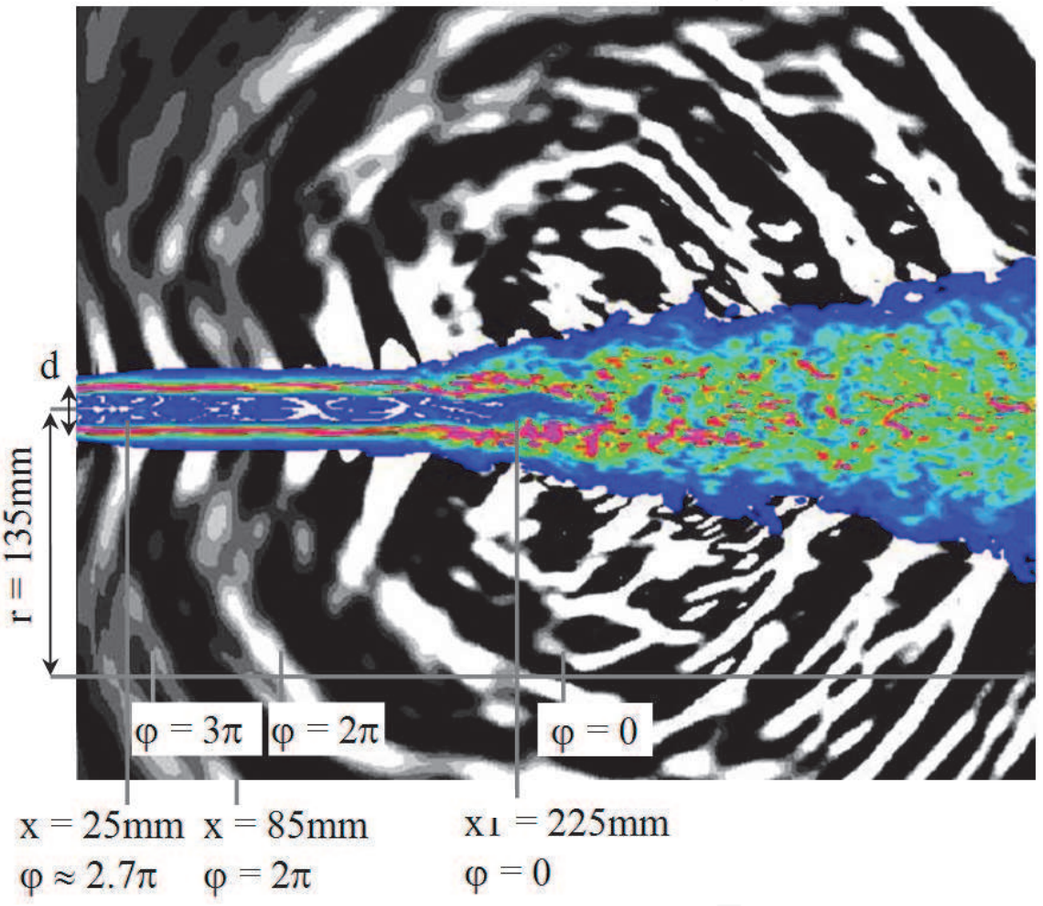

Fig. 13. Results of numerical simulation of the acoustic field (Bodony, 2005) in comparison with experimental data on the phase shift in configuration 1.

6.2 T-313 wind tunnel

6.2.1 Laser radiation intensity fluctuations

Figure 14 shows the spectra of intensity fluctuations $U(f)$ of the laser radiation propagating in the supersonic flow in T-313 over the model wing as shown in Fig. 4. It can be seen from Fig. 14 that in the region of high frequencies $f \geq f_2$ the spectra is qualitatively close to the spectra of intensity fluctuations obtained in T-326 (Fig. 7). As the angle of attack increases,

fluctuations become much stronger in the region of low frequencies and more slightly intensify in the region of the high-frequency maximum f_2. Figure 14b depicts the spectra normalized to their values at the frequency of the maximum f_2 as functions of the frequency normalized to f_2.

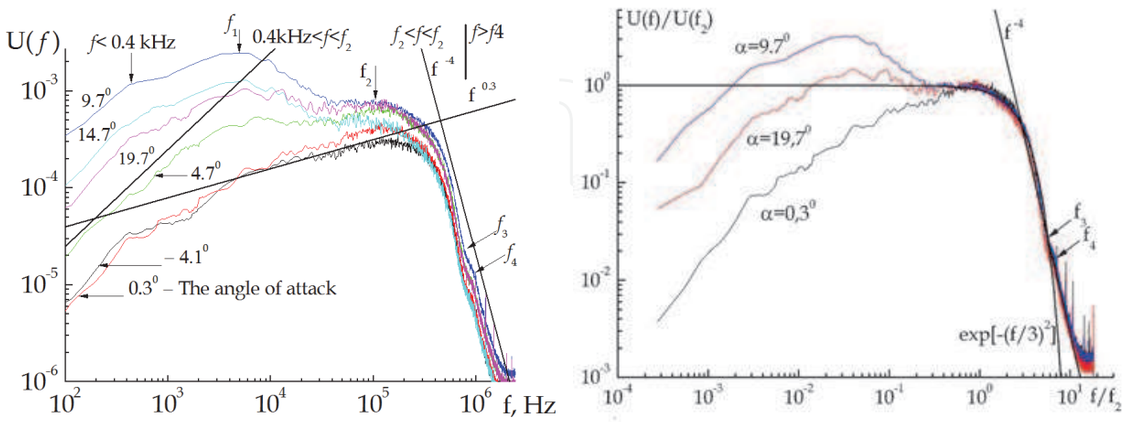

a b

Fig. 14. Spectra of intensity fluctuations at different angles of attack (a) and normalized spectra (b).

Low-frequency fluctuations are caused by the effect of acoustic noise generated by the supersonic flow above the model. The wavelength of the generated sound can be estimated as $\Lambda \approx V_c/f_1$, where $V_c \approx 20.1 \cdot T^{1/2} = 200 - 250$ m/s is the sound speed at the flow temperature. In this case $\Lambda \approx 3$-6 cm.

The dependence of the relative variance of intensity fluctuations in the probing laser beam on the angle of attack is shown in Fig. 15. In this figure, the vertical axis is divided into two sections having different scales for the presentation of significantly different values. It can be seen from the figure that incoming flow is actually laminar, and the relative variance of intensity fluctuations is only $\sigma^2 \sim 3 \cdot 10^{-5}$ in this case. Above the wing, the relative variance is four orders of magnitude higher, thus indicating the significant turbulization of the flow above the model.

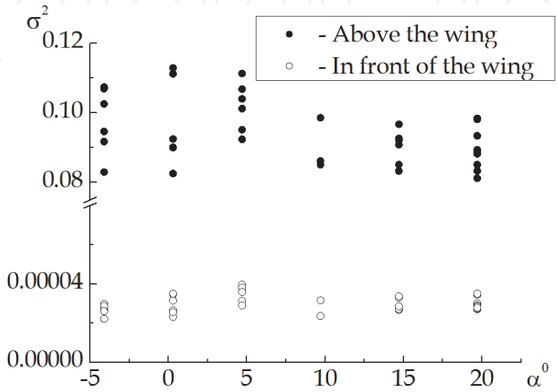

Fig. 15. Relative variance of intensity fluctuations at different angles of attack.

6.2.2 Fluctuations of the laser beam propagation direction

The spectra of fluctuations of the laser beam propagation direction in the supersonic flow in T-313 above the model were measured by a quadrant detector (QD) by the scheme shown in Fig. 4.

It follows from the analysis of the measurement results that the spectra of beam propagation direction fluctuations along the x axis have a peak near 19-24 kHz, while those along the y axis have a peak near 16-26 kHz. The frequency of the spectral maximum depends on the angle of attack. It is minimal at the negative angle of attack, maximal at $\alpha = 0.3°$, and decreases slightly with an increase in the angle of attack (Fig. 16a). Vertical bars in the figure show the spread in values.

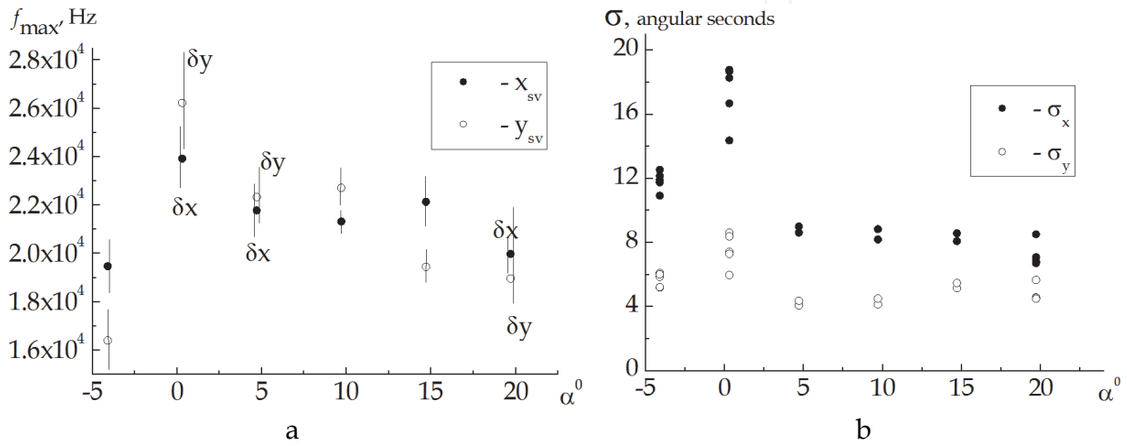

Fig. 16. Dependence of the frequency of the spectral maximum (a) and the standard deviation (b) of fluctuations of the laser beam propagation direction on the angle of attack $\alpha°$.

In the high-frequency region $f > f_{max}$, the spectra of random beam displacements decrease as $\sim f^{-4/3}$ in the horizontal direction (x axis) and as $\sim f^{-(0.6\text{-}0.8)}$ in the vertical direction (y axis). The difference of the slopes is indicative of the nonisotropic fluctuations of the probing beam propagation direction in the horizontal and vertical directions. Fluctuations in the vertical direction are roughly halved compared to those in the horizontal direction and weakly depend on the angle of attack (Fig. 16b). The variance of random displacements of the beam is maximal at the angle of attack $\alpha = 0.3°$, that is, at the maximal flow speed above the wing.

The frequency of the maximum in the spectrum of laser beam image jitter recorded by the dissector tube (Fig. 4) is 250-300 Hz along the horizontal axis and 200-270 Hz along the vertical axis at angles of attack ≤ 15° and increases sharply up to 500 Hz at an angle of attack of 19.7°. These fluctuations are possibly caused by the vibration of the wing under the effect of the incoming flow. The standard deviation of the image jitter is 12-17 arc sec. and is maximal at an angle of attack of ~15°.

7. Conclusions

Thus, the experimental results obtained show that the spectra of intensity fluctuations of the probing laser beam has roughly the same form both in the case of the supersonic jet

generated by the T-326 jet unit and in the case of a model wing blown by a supersonic flow in T-313. The maximum of turbulent intensity fluctuations in the both cases falls on frequencies in the region of 50 kHz and higher. The estimates based on the Kolmogorov—Obukhov model of developed turbulence show that the structure characteristic of the refractive index in the studied supersonic flows is several orders of magnitude higher than C_n^2 in the atmosphere.

The optical model of turbulence developed on the basis of Fluent-6 allows one to simulate the propagation of a probing laser beam in supersonic flows with arbitrary geometric and thermodynamic parameters. The results of simulation and reconstruction of optical model parameters from simulated data on the probing of a supersonic jet in T-326 are close to the experimental findings.

From the results of acoustic measurements as well as from the probing laser beam intensity fluctuations, it follows that the supersonic jet generates sound. The source of sound lies in the region of the transition from the supersonic flow speed to the subsonic one. For the jet unit of the T-326 wind tunnel, the sound source is on the jet axis at a distance of 225 mm from the nozzle. With the distance from the source, the generated acoustic wave becomes close to a spherical one.

The work was financially supported in part by the Russian Foundation for Basic Research, grant 11-08-01059.

8. References

Abbrecht, H.-E., Damaschke, N., Borys, M. & Tropea, C. (2003). *Laser Doppler and Phase Doppler Measurement Techniques. Series: Experimental fluid Mechanics.* Springer-Verlag, ISBN: 978-3-540-67838-0, Berlin.

Bodony, D.J. (2005). *The prediction and understanding of jet noise.* Center for Turbulence Research Annual Research Briefs, pp.367-377.

Canuto, V.M. (1997). Compressible Turbulence. *The Astrophysical J.*, V.482, No.2, pp. 827-851, ISSN: 0004-6256.

Dmitriev, D.I., Ivanov, I.V., Sirazetdinov, V.S. & Titterton, D.H. (2004). Statistics of structural state fluctuations of a laser beam disturbed by a jet of aircraft engine. *Atmospheric and Oceanic Optics*, Vol. 17, No.01, pp.39-45, ISSN 0235-6880.

Fomin, N.A. (1998). *Speckle Photography for Fluid Mechanics Measurements. Series: Experimental Fluid Mechanics.* Springer-Verlag, ISBN: 978-3-540-63767-7, Berlin.

Garkusha, V.V., Sobstel, G.M., Surodinn, S.P., Yakovlev, V.V., Gilev, V.M, Zapryagaev, V.I. & Pishchik, B.M. (2009) Automatic Control System for Technological Processes of a Turboblower Station. *Problems of Informatics.* No.3(4), pp. 85-93, ISSN 2073-0667.

Gurvich, A.S., Kon, A.I., Mironov, V.L. & Khmelevtsov, S.S. (1976). *Laser Radiation in the Turbulent Atmosphere*. Nauks. Moscow.

Joia, I.A., Perkins, R.J., Uscinski, B.J., Balmer, G., Jordan, D. & Jakeman, E. (1995). Optical properties of a planar turbulent jet. *Appl. Opt.*, Vol.34, No. 30, pp.7039-7053, ISSN: 1559-128X.

Joia, I.A., Uscinski, B.J., Perkins, R.J., Balmer, G., Jordan, D., & Jakeman, E. (1997). Intensity fluctuations in a laser beam due to propagation through a plane turbulent jet. *Waves in Random Media,* Vol.7, No. 2, pp.169-181, ISSN: 1745-5030.

Kandidov, V.P. (1996) Monte Carlo Technique in Nonlinear Statistical Optics *Physics-Uspekhi* V.166, No.12, pp. 1309-1338, ISSN: 1063-7869.

Kuznetsov, V.M. (2008) *Principles of Theory of Noise of Turbulent Jets.* Fizmatlit, ISBN: 9785922109703, Moscow.

Launder, B.E. & Spalding D.B. (1972) *Lectures in Mathematical Models of Turbulence*. Academic Press, London, England.

Monin, A. S. & Yaglom, A.M. (1971) Statistical fluid mechanics, vol.1. Ed. J. Lumley. MIT Press, Cambridge, MA.

Monin, A. S. & Yaglom, A.M. (1975) Statistical fluid mechanics, vol.2. Ed. J. Lumley. MIT Press, Cambridge, MA.

Pade, O. (2001). Models of turbulence for aero-optics application. *Proceedings SPIE*. Vol.4419, pp.494-498, ISBN: 9780819441263.

Pade, O., Frumker E. & Rojt P.I. (2004). Optical distortions caused by propagation through turbulent shear layers. *Proceedings SPIE*. Vol.5237, pp.31-38, ISBN: 9780819451200.

Pade, O. (2004). Optical propagation through turbulent jets. *Proceedings SPIE*. Vol.5572, pp. 24-33, ISBN: 9780819455192.

Pade, O. (2006). Optical propagation through Shear Layers. *Proceedings SPIE*. Vol.6364, p.63640E, ISBN: 9780819464590.

Raffel, M., Willert, C., Wereley, S.T. & Kompenhans, J. (2007). Particle image velocimetry: A practical guide. Springer-Verlag, ISBN: 978-3-540-72307-3, Berlin.

Shih, T.-H., Liou, W. W., Shabbir, A. & Zhu, J. (1995) A New k-ε Eddy-Viscosity Model for High Reynolds Number Turbulent Flows - Model Development and Validation. *Computers Fluids*, Vol.24, No.3, pp.227-238, ISSN: 0045-7930.

Sirazetdinov, V.S., Dmitriev, D.I., Ivanov, I.V. & Titterton, D.H. (2001) Effect of turbo-engine jet on laser radiation. Part 2. Random wandering of disturbed beam. *Atmospheric and Oceanic Optics*, V. 14, No.10, pp.830-834, ISSN: 0235-6880.

Smits, A.J. & Dussauge, J.-P. (1996). *Turbulent shear Layers in supersonic flow.* American Institute of Physics Press. USA.

Tatarskii,V.I. (1961) *Wave propagation in a turbulent medium.* Translated from the Russian by R.A. Silverman. McGraw-Hill, New York, Toronto, London,. Second edition: Dover Publications, New York, 1967.

Tatarskii, V.I. (1971) The effects of the turbulent atmosphere on wave propagation. Translated from the Russian by the Israel Program for Scientific Translations, Jerusalem,. Available from the U.S. Dept. of Comm., Nat. Tech. Inf. Serv., Springfield, VA, 22151.

Yakhot, V. & Orszag, S.A. (1986) Renormalization Group Analysis of Turbulence: I. Basic Theory. *Journal of Scientific Computing*, Vol.1, No.1, pp.1-51, ISSN: 0885-7474.

Yoshizawa, A. (1995). Simplified statistical approach to complex turbulent flowsand ensemble-mean compressible turbulence modeling *Phys. Fluids*. V.7, No.12, pp.3105-3117, ISSN: 1070-6631.

Zuev, V.E., Banakh, V.A. & Pokasov, V.V. (1988). *Optics of the Turbulent Atmosphere.* Gidrometeoizdat. ISBN: 5286000533, Leningrad.

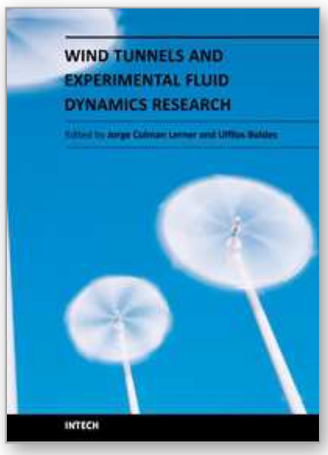

Wind Tunnels and Experimental Fluid Dynamics Research

Edited by Prof. Jorge Colman Lerner

ISBN 978-953-307-623-2
Hard cover, 709 pages
Publisher InTech
Published online 27, July, 2011
Published in print edition July, 2011

The book â€œWind Tunnels and Experimental Fluid Dynamics Researchâ€ is comprised of 33 chapters divided in five sections. The first 12 chapters discuss wind tunnel facilities and experiments in incompressible flow, while the next seven chapters deal with building dynamics, flow control and fluid mechanics. Third section of the book is dedicated to chapters discussing aerodynamic field measurements and real full scale analysis (chapters 20-22). Chapters in the last two sections deal with turbulent structure analysis (chapters 23-25) and wind tunnels in compressible flow (chapters 26-33). Contributions from a large number of international experts make this publication a highly valuable resource in wind tunnels and fluid dynamics field of research.

How to reference

In order to correctly reference this scholarly work, feel free to copy and paste the following:

Viktor Banakh, Dmitri Marakasov, Ruvim Tsvyk and Valeri Zapryagaev (2011). Study of Turbulent Supersonic Flow Based on the Optical and Acoustic Measurements, Wind Tunnels and Experimental Fluid Dynamics Research, Prof. Jorge Colman Lerner (Ed.), ISBN: 978-953-307-623-2, InTech, Available from: http://www.intechopen.com/books/wind-tunnels-and-experimental-fluid-dynamics-research/study-of-turbulent-supersonic-flow-based-on-the-optical-and-acoustic-measurements

INTECH
open science | open minds

InTech Europe
University Campus STeP Ri
Slavka Krautzeka 83/A
51000 Rijeka, Croatia
Phone: +385 (51) 770 447
Fax: +385 (51) 686 166
www.intechopen.com

InTech China
Unit 405, Office Block, Hotel Equatorial Shanghai
No.65, Yan An Road (West), Shanghai, 200040, China
中国上海市延安西路65号上海国际贵都大饭店办公楼405单元
Phone: +86-21-62489820
Fax: +86-21-62489821

IntechOpen